Environ Earth Sci (2017) 76:412
DOI 10.1007/s12665-017-6747-x

ORIGINAL ARTICLE

Derivation of fractional urban signals in better capturing urbanization process

Ronghan Xu[1] · Yonghong Hu[2] · Hao Gao[1] · Zharong Pan[3]

Received: 31 August 2016 / Accepted: 2 June 2017 / Published online: 12 June 2017

Abstract Rapid urbanization has changed land use and urban structure in China and therefore greatly modified land surface properties and land–atmosphere interactions, causing further local and regional climate change. Climate model simulation and urbanization process analysis are usually limited by poor accuracy of coarse-resolution land use/cover products employed in regional climate models. This study sought to identify better urban representation from Landsat images and monitor urban expansion by change detection of spatial patterns and urban fractions in southeastern coastal region of China. We used the improved normalized indices-based method to classify urban and built-up areas from Landsat images in Jiading District, Shanghai. Classification results were evaluated at both the pixel scale and the model grid scale, with overall accuracy of 88% and k coefficient of 0.76. Moreover, urbanization process over the Guangzhou–Foshan–Dongguan area was examined from 2000 to 2009. We aggregated the original results of urban classification data from Landsat images as fractional cover information in 1-km grids. The total fractional urban change in 2000–2005 (10.65%) was approximately three times greater than in 2005–2009 (3.38%). We also compared the fractional cover of urban expansion with the corresponding period of MODIS land cover products. It showed that existing land cover products in models had deviations and could not capture well the underlying conditions and urbanization process. Different fractional covers of urban scenarios were expected to provide better inputs for accurate modeling of critical environmental feedbacks over expanding urban clusters.

Keywords Urban · Satellite · Normalized index · Fractional cover · Regional climate models

Introduction

Urban areas facilitate intensified human activities, although they currently cover less than 1% of the Earth's surface (Gong et al. 2013). In the wake of rapid economic development, urbanization has been attributed to the accelerating integration of developing areas in East Asia into the world economy, which has involved dramatic changes in land use and urban structure in China (Dick and Rimmer 1998). Urbanization rate of China has increased from 19.4 to 55.74% during 1980–2014 as revealed by the census data from the National Bureau of Statistics of China (http://www.stats.gov.cn).

Urbanization has permanently converted large areas of cropland and natural vegetation to impervious urban land, resulting in the changes to land surface properties including land use/cover, surface albedo, and surface roughness et al. (Kalnay and Cai 2003; Foley et al. 2005; Normile 2008; Hu et al. 2015b). This transformation in urban areas has greatly altered energy and water exchange in land–atmosphere interactions and boundary layer processes over urban canopies and downstream areas, causing further local and regional climate change (Crawford et al. 2001; Ren et al.

✉ Ronghan Xu
tsuicas@163.com

[1] National Satellite Meteorological Center, China Meteorological Administration, Beijing 100081, China

[2] Key Laboratory of Digital Earth Science, Institute of Remote Sensing and Digital Earth, Chinese Academy of Sciences, Beijing 100094, China

[3] General Institute of Water Resources and Hydropower Planning and Design, MWR, Beijing 100120, China

2008; Fernando et al. 2012; Fischer et al. 2012; Peng et al. 2012). Global temperatures have increased since pre-industrial times; however, the trends and magnitudes of climate warming induced by urbanization on different spatial scales are still controversial (Stocker et al. 2013).

To investigate the accurate impacts of urbanization on climate change, more and more regional climate models have been implemented by employing different land use change scenarios. However, recent studies indicate that accurate representation of urban land use is important but poorly captured in current climate models (Oleson et al. 2008; Gao and Jia 2013; Jia et al. 2015). The default land cover data sets used in regional climate models, e.g., Weather Research and Forecasting (WRF) model, are at a coarse resolution of 1 km. The urban and built-up areas within those data sets are not very accurate in capturing surface properties due to limits in spatial resolution and classification algorithm, which would result in deviations in model simulation (Ge et al. 2007; Friedl et al. 2010; Sertel et al. 2010). These urban data are not up-to-date and have low Cohen's kappa values for regions in experiencing rapid urbanization process such as Southeast and East Asia (Potere et al. 2009). Meanwhile, researches showed that the better representations of urban features can directly improve model outputs. For example, Sertel et al. (2010) found that simulations with the new land cover data from Landsat led to more reasonable temperature than with the default land cover data employed in WRF model. Root-mean-square errors for the Landsat-derived data were between 2.1 and 3 °C, whereas for the existing land cover data are between 2.9 and 7.1 °C. Therefore, the deviation of urban land use/cover data declines the results of climate modeling and probably results in the uncertainty of climate warming trends and magnitude by urbanization.

Integration of human and earth system models for climate change impact assessment requires consistent projections of urban extent and accurate representation of urban intensity. The nature of urban built-up areas, such as the size, shape, intensity, and spatial context, is a key parameter of climate models (Jackson et al. 2010). Many researchers have made use of remote sensing imagery to distinguish urban lands from non-urban lands. To interpret remotely sensed data for urban derivations, methods range from pure interpretation, semiautomated and fully automated have been proposed (Sun et al. 2013). Pure interpretation started with conventional multispectral visual classification, which normally has less than 80% accuracy (Xu 2007). Semiautomated methods, such as supervised classification by the maximum likelihood classifier, have accuracy depending on subjective training samples. Due to spectral confusion of the heterogeneous urban built-up land class, classification of a multidate, multiband image would be difficult for the most common classification algorithm (Schneider et al. 2005; Hu et al. 2015a). Many studies combined different methods to improve the urban extraction. Fully automated approaches, e.g., combination of different indices without manual thresholding, have the advantages of quickly and more objectively processing data and thus are easy replicated (He et al. 2010). On the one hand, urban landscapes are typically composed of features, such as buildings, concrete pavements, which are much smaller than the grid resolution of regional climate models. Moreover, urban mapping accuracies increase with increasing spectral sensor resolution (Herold and Roberts 2010). Thus, we used Landsat data to map urban extent, because of their long-term digital archives as well as the fine spatial resolution for capturing urban characteristics in models (Bagan and Yamagata 2012; Weng 2012; He et al. 2013). On the other hand, urban intensity can be represented by fractional urban signals aggregated by the original results of urban classification data from Landsat images. This fractional urban land cover may capture well the urbanization process and provide detailed dynamic information.

Therefore, the purpose of this paper is to identify better urban representation than the existing urban data in regional climate models and consequently to provide better inputs for accurate modeling of critical environmental feedbacks over expanding urban clusters. We classified urban and built-up areas from Landsat images based on normalized indices and aggregated the original results of urban classification data from Landsat images as fractional cover information in 1-km grids. Moreover, the urbanization process over the Guangzhou–Foshan–Dongguan area was examined from 2000 to 2009 by change detection of spatial patterns and urban fractions. We also evaluated the accuracy or deviations of existing urban land cover products to examine their limitations in climate model simulation and urbanization process analysis.

Study area

Southeastern coastal region of China has been experiencing rapid urbanization and economic growth by government directives (Seto et al. 2002). Fringe area and satellite towns caused by rapid urbanization process made more mosaic land surface characterization in this region. We chose two representative areas around Shanghai and Guangdong over southeastern coastal region of China (Fig. 1). One was focused on the center of Jiading District (31°23′N, 121°15′E), northwest of Shanghai (Fig. 1a). It was confined to a 9 km × 9 km test site with a round moat and a ring road in the center. The other was located in the Guangzhou–Foshan–Dongguan area (GFD), confined to a 79 km × 93 km window (columns and rows) (Fig. 1b).

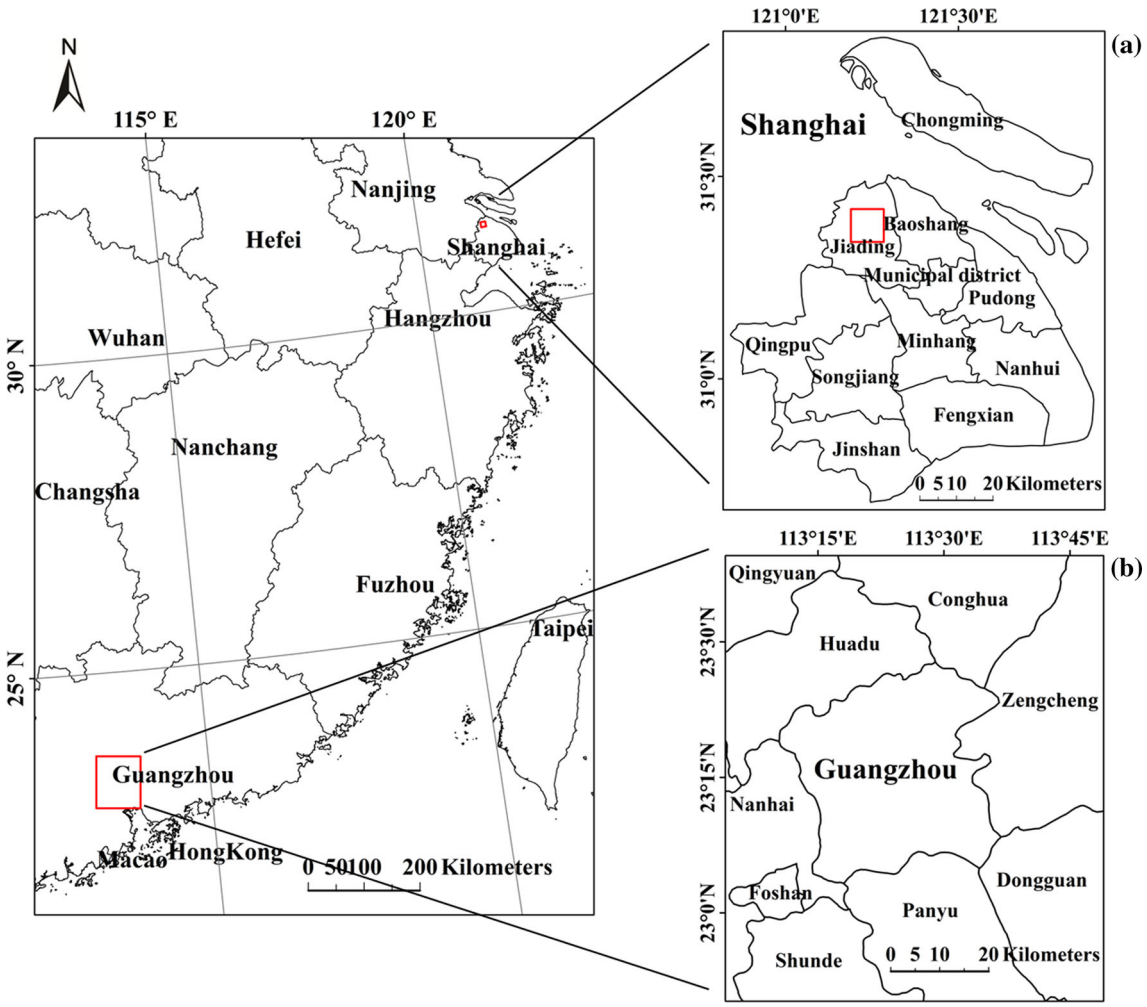

Fig. 1 Location of this study in southeastern coastal region of China: **a** *the red rectangle* is the test site located in the Jiading District, Shanghai; **b** the case study area for urban fractional change detection, located in the Guangzhou–Foshan–Dongguan area

Data and methods

Data sets for urban land cover derivation

Landsat images

Cloud-free and high-quality Landsat TM/ETM + data (Table 1) covering the above areas were collected from the USGS government website (http://earthexplorer.usgs.gov/). The Landsat data were geometrically rectified according to the Universal Transverse Mercator projection at 30 m × 30 m resolution, using second-order polynomial and bilinear interpolation. Ground control points were selected from intersections of river channels and roads, and RMSEs for geo-correction were less than 1.5 pixels. In addition, some auxiliary data were also collected to

Table 1 MODIS land cover product and Landsat TM/ETM + images used in this study

Satellite	Landsat TM/ETM	Terra MODIS
Location and time	P118/R38, April 27, 2000	
	P122/R44 November 1, 2000, November 23, 2005, December 4, 2009	H28V06 2001 2005 2009
Spatial resolution	30 m	500 m
Method for urban land identification	Normalized indices-based classification (original urban land fractions)	Decision tree classification (fractional urban land >50%)
Definitions of urban area	Urban area or urban-related instructions	Buildings and other man-made structures

validate classification results, including a 1:50,000 scale topographic map, historical images from Google Earth, and field investigations.

Existing land cover products employed by climate models

The 500-m C5 MODIS land cover product (MCD12Q1, Friedl et al. 2010) in 2001, 2005, and 2009 (Table 1) was collected from the MODIS land team (http://modis-land.gsfc.nasa.gov/). For comparison with Landsat-derived urban land cover data, MODIS tiles over study areas of these products were resampled by the nearest neighbor method and reprojected under the datum of WGS84 by the MODIS Reprojection Tool (MRT, http://lpdaac.usgs.gov/tool/modis_reprojection_tool). The International Geosphere-Biosphere Programme (IGBP) classification scheme was chosen for urban-class derivation and the analysis of the reprocessed data. The urban and built-up category (class 13) was defined as the area covered by buildings and other man-made structures (Friedl et al. 2002). The MODIS products were reclassified into urban (class 13) and non-urban (other classes) categories to facilitate the subsequent process.

Normalized Indices-based Urban Built-up Areas Mapping

The normalized difference vegetation index (NDVI) and other normalized indices are widely used in environmental and climatic related studies. With respect to urban area classification, Zha et al. (2003) proposed the normalized difference built-up index (NDBI) to map urban built-up areas. First, continuous (c) NDVI and NDBI images were obtained by spectral responses of pixels in the following equations.

$$\mathrm{NDVIc} = (\mathrm{NIR} - \mathrm{RED})/(\mathrm{NIR} + \mathrm{RED}) \quad (1)$$

$$\mathrm{NDBIc} = (\mathrm{MIR} - \mathrm{NIR})/(\mathrm{MIR} + \mathrm{NIR}) \quad (2)$$

Second, the derived NDVIc and NDBIc were recoded to create binary NDVI and NDBI image with 1 for all pixels having positive value and 0 for all remaining pixels of negative value. Finally, the urban and built-up areas were extracted by taking only positive difference values of binary (b) NDBI and NDVI images.

$$\mathrm{Ub} = \mathrm{NDBIb} - \mathrm{NDVIb} > 0 \quad (3)$$

However, the binary NDBI and NDVI images were recoded under the assumption that all positive values of continuous NDBI and NDVI images should indicate built-up areas and vegetated areas, respectively. Thus, this mapping method is unable to separate urban areas from patches with low fractions of natural vegetation and bare lands.

Xu (2007) proposed an urban mapping method by a logic calculation, which involved three indices including NDBI, modified normalized difference water index (MNDWI), and soil adjusted vegetation index (SAVI). The continuous images of MNDWI and SAVI can be calculated by the following equations.

$$\mathrm{MNDWIc} = (\mathrm{GREEN} - \mathrm{MIR})/(\mathrm{GREEN} + \mathrm{MIR}) \quad (4)$$

$$\mathrm{SAVIc} = (1 + \mathrm{L})(\mathrm{NIR} - \mathrm{RED})/(\mathrm{NIR} + \mathrm{RED} + \mathrm{L}) \quad (5)$$

where L is the correction factor for soil background brilliance, and the value of L is from 0 to 1 and set to 0.5 for urban areas.

The logic calculation stated that if the values of pixels in continuous NDBI images were greater than both values in continuous MNDWI and SAVI images, then the pixels were considered as built-up category.

$$\mathrm{Uc} = (\mathrm{NDBIc} > \mathrm{SAVIc})\mathrm{AND}(\mathrm{NDBIc} > \mathrm{MNDWIc}) \quad (6)$$

Here, we improved urban areas mapping method based on Uc. By examining the spectral reflectance of 100 representative pixels of urban built-up and non-built-up areas (e.g., vegetation and water), it has been found that built-up areas have an increase in reflectance from green band to red band (band 2 and band 3 in Fig. 2). The red band is used for detection of chlorophyll (i.e., vegetation), which absorbs high in the red wavelengths, as well as for the observation of roads and bare lands, which reflect highly in the red band. The green band is mainly used to distinguish vegetation from background categories, as vegetation reflects highly in the green band. Taking advantage of a normalized calculation, an urban index can be expressed by the standard difference between these two bands.

$$\mathrm{UIc} = (\mathrm{RED} - \mathrm{GREEN})/(\mathrm{RED} + \mathrm{GREEN}) \quad (7)$$

Based on the above spectral characteristic, the improved method involved four indices including NDBIc, MNDWIc, SAVIc, and UIc. The four indices were used as four bands of a new image. For the new image, in addition to the band characteristics described by Uc, the positive value of UIc could help to further capture weak urban signals, especially in those areas of low fractional vegetation. The Integrated Urban Index (IUI) approach was proposed to segment urban built-up areas from other land types using an improved logic calculation.

$$\mathrm{IUI} = (\mathrm{NDBIc} > \mathrm{SAVIc})\mathrm{AND}(\mathrm{NDBIc} > \mathrm{MNDWIc}) \mathrm{AND}(\mathrm{UIc} > 0) \quad (8)$$

The IUI approach and existing mapping methods (Ub and Uc) were applied and evaluated in Jiading District by logic tree operation to identify urban built-up and non-urban classes.

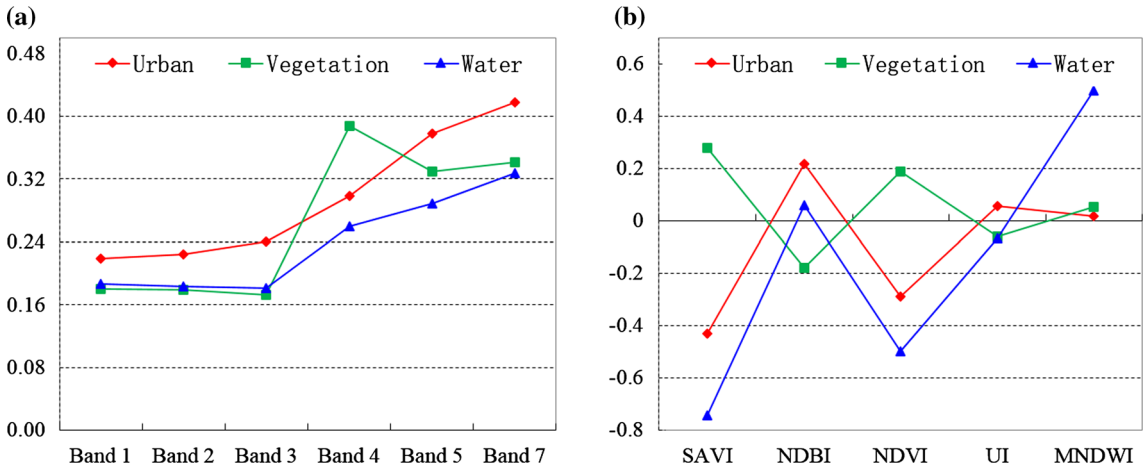

Fig. 2 **a** Spectral reflectance of urban built-up, vegetation, and water in different bands, taking the Jiading Landsat ETM + image as an example, **b** spectral features of different normalized indices represented by urban built-up, vegetation, and water

Assessment methods

Accuracies of the IUI against existing methods (Ub and Uc) were performed at both the pixel scale and the model grid scale of 1 km. At the pixel scale, based on historical images from Google Earth and field investigation, 100 random samples for built-up areas and 100 for non-built-up areas for each method were created by Python code to validate our results. Four commonly used measures, namely the overall accuracy, the kappa (κ) coefficient, omission error, and commission error, were calculated from the confusion matrix to reveal the accuracies of the IUI against existing methods. The overall accuracy is computed by dividing the total number of correctly classified pixels by the total number of reference pixels. The κ is calculated by multiplying the total number of pixels in all the ground truth classes (N) by the sum of the confusion matrix diagonals (x_{kk}), subtracting the sum of the ground truth pixels in a class times the sum of the classified pixels in that class summed over all classes ($x_{k\Sigma}x_{\Sigma k}$), and dividing by the total number of pixels squared minus the sum of the ground truth pixels in that class times the sum of the classified pixels in that class summed over all classes by the following equation.

$$\kappa = \frac{N\sum_{k} x_{kk} - \sum_{k} x_{k\Sigma}x_{\Sigma k}}{N^2 - \sum_{k} x_{k\Sigma}x_{\Sigma k}} \quad (9)$$

The omission error represents pixels that belong to the ground truth class, but the classification technique has failed to classify them into the proper category. The commission error represents pixels that belong to another class that are labeled as belonging to the class of interest.

At the model grid scale, urban fractions were calculated by the algebraic proportions of urban and built-up areas within the given landscape unit. Firstly, we aggregated the original results of urban classification data from Landsat images as fractional cover information in 1-km grids. Then, we chose three grids as exemplars with 990 m × 990 m window to represent urban fractions at the model grid scale for different development levels, i.e., from rural, to urban–rural fringe, and to urban. The 990 m is chosen because it can be divided by 30 m (the resolution of Landsat data) and comparable to 1 km. Next, the urban and built-up areas for corresponding locations of grids from QuickBird imagery were delineated by manual interpretation and on-screen digitization. The proportions of these outlined urban areas within grids were computed as urban fractions for evaluation of reference. Thus, urban fractions aggregated from Landsat and QuickBird images were compared and examined.

Detection of urban expansion

A framework for change detection of urban expansion at the model grid resolution of 1 km based on IUI was created. Firstly, the IUI approach was applied to Guangzhou–Foshan–Dongguan area to map urban areas based on Landsat images in 2000, 2005, and 2009, respectively. The 30-m IUI-based urban areas were derived for the three periods. Second, square grids at 1-km spatial resolution were created to cover the boundaries of the study area. Next, urban land classification results were aggregated to a 1-km resolution by calculating proportions of urban areas within grids. Thus, fractional covers of urban land in 1-km grids were derived for these years. We examined urban expansion by change detection of spatial pattern and urban fractions. The interval of 0.2 was taken as an example to analyze development of urban intensity from 2000 to 2009. At last, we overlaid and compared with MODIS urban land

cover to examine accuracy of existing land cover data in climate models.

Results

Comparison of urban and built-up areas classifications

Urban areas were derived by Ub, Uc, and IUI approaches from Landsat ETM + image taken on April 27, 2000, located in Jiading District, Shanghai (Fig. 3). The IUI result for the test site was in high agreement with the expected urban morphology in the original Landsat imagery. The Ub result only delineated the outline of urban and built-up area, neglecting details within the city. The Uc result represented some information of interior urban, but it described little in area of low vegetation density within the city. Thus, the IUI approach is a better alternative than existing methods for patchy urban area detection, because it not only delineated the urban outline but also classified urban land from the inner mosaic land surface.

Accuracy

Pixel scale

The overall accuracy of IUI approach was 88% (Table 2), greater than Ub (70.5%) and Uc (83.5%). The values of the κ coefficient for Ub, Uc, and IUI were 0.41, 0.67, and 0.76, respectively. Moreover, Ub and Uc methods had higher commission errors than the IUI approach, incorrectly assigning some non-urban areas to urban class (see the area in the red rectangle in Fig. 3). The results demonstrated that the IUI was able to capture detailed urban land use with higher accuracy than existing methods when applied simultaneously in the same context.

Model grid scale

Grids at around 1 km were chosen to evaluate the ability of IUI method to capture urban signals in various cases. Grid I, II, and III, located in the northwest of the Jiading District, were taken as exemplars to represent urban fractions of different development levels in this region (Fig. 4), i.e., from rural, to urban–rural fringe, and to urban. Results showed that urban extent delineated by Ub was in the least agreement with the expected urban morphology from high-resolution QuickBird and pan-sharpened images. Urban fractions of each grid using Ub, Uc, and IUI methods, as well as corresponding locations from the QuickBird image, are compared (Table 2). The values of urban fractions calculated from the IUI approach were more comparable to those from the QuickBird image than Ub and Uc methods. For grid III, urban fraction using Ub was 100%; however, there were obviously non-urban areas in both the QuickBird and pan-sharpened images. The results indicated that the urban fractions from the IUI had a higher accuracy than existing methods when compared at the 1-km scale. IUI can effectively capture accurate fractional urban signals for different development levels of urbanization and therefore better estimate urban fractions at coarse resolution for climate models.

Changes in fractional urban lands under urbanization in the GFD area

Spatial pattern

The spatiotemporal patterns of urban fractions over the Guangzhou–Foshan–Dongguan area at the 1-km scale in 2000, 2005, and 2009 are shown in Fig. 5. From 2000 to 2005, the development of satellite towns was prevalent in the north and southeast, such as Qingyuan and Huadu. From 2005 to 2009, apart from satellite towns in Zengcheng, the main change in urban fraction resulted from increasing intensity of core areas, i.e., Guangzhou, Foshan, and Dongguan. Results showed that urban development in this region has been directed out of the core areas to nearby towns, leading to a poly-nucleated urban form. Multidirectional satellite towns emerged and located in the periphery from the core city. The connections between the core area and satellite towns are covered by low intensity of urban fractions.

Urban fractions

Change detection of urban fractions at the model grid resolution was applied by IUI for detailed urban expansion in GFD area. Urban fractions were analyzed and summarized at intensity of 0.2 (Table 3). Urban fractions in the intensity of 0.6–1 increased from 2000 to 2009. The 0.6–0.8 intensity increased twice more in 2000–2005 (5.10%) than in 2005–2009 (1.71%), whereas the 0.8–1 intensity increased comparatively in 2005–2009 (1.67%) and in 2000–2005 (1.92%). In contrast, urban fractions in the intensity of 0–0.4 decreased from 2000 to 2009, indicating denser urban canopy and reduced gaps among urban clusters in past decade. The 0–0.2 intensity decreased much more in 2000–2005 (7.73%) than in 2005–2009 (1.27%). It is noteworthy that urban fractions in the intensity of 0.4–0.6 increased 3.63% in 2000–2005 and then decreased 0.41% in 2005–2009. From 2000 to 2005, we found that the maximum increase in urban fractions in this region was in the intensity of 0.6–0.8, whereas the maximum decrease was in 0–0.2. From 2005 to 2009, results showed that the maximum decrease in urban fractions was in the intensity

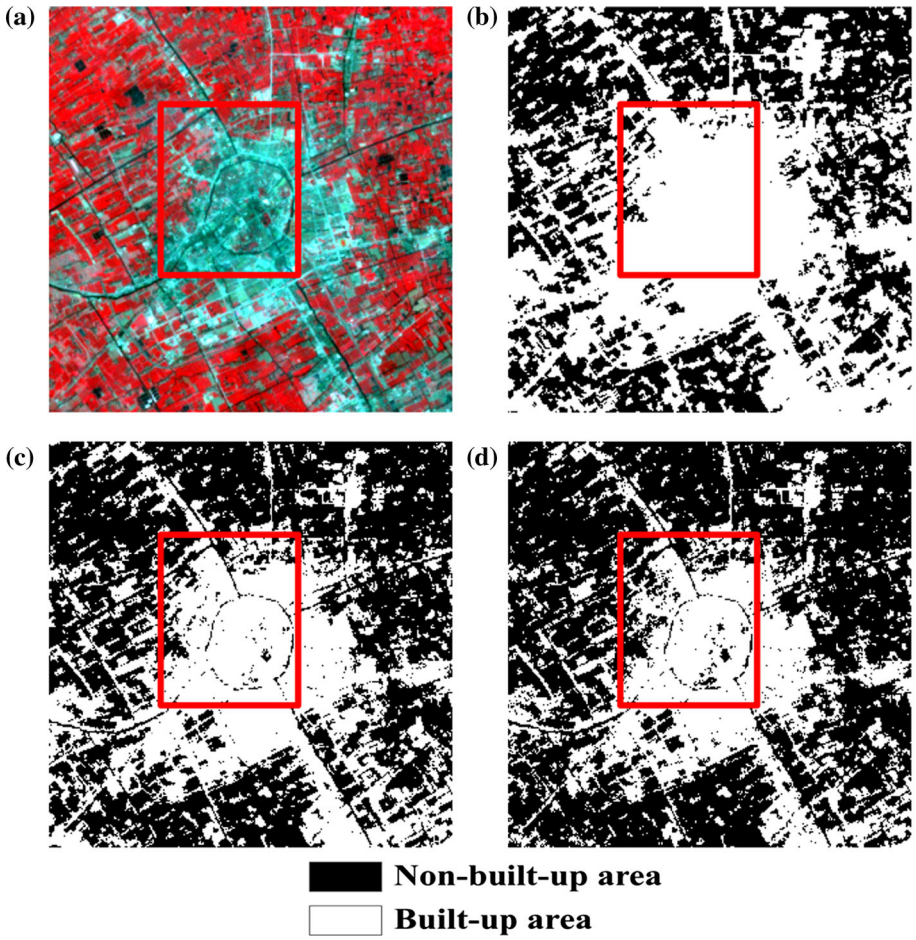

Fig. 3 Comparison of results by IUI and existing methods: **a** the false color composition (red:NIR, green:red and blue:green) of the Landsat ETM + image taken on April 27, 2000, located in Jiading District, Shanghai; **b**–**d** classification images of urban and built-up areas by methods of Ub, Uc, and IUI, respectively; *the red rectangle* in each panel shows where existing methods of Ub and Uc produced obvious commission error, incorrectly assigning some non-built-up areas as urban class

Table 2 Accuracy assessments of IUI and existing methods at both the pixel scale and the model grid scale of 1 km

Methods	Stratified random sampling at the pixel scale			
	Overall accuracy (%)	κ Coefficient	Omission error (%)	Commission error (%)
Ub	70.50	0.41	6.38	56
Uc	83.50	0.67	7.59	27
IUI	88.00	0.76	5.81	19
Grids	Urban fractions at the model grid scale			
	Ub (%)	Uc (%)	IUI (%)	Quick bird (%)
I	38.84	26.45	18.18	20.56
II	77.96	63.54	47.75	48.35
III	100	90.91	84.21	87.45

of 0.2–0.4. Overall, the total fractional urban change in 2000–2005 (10.65%) was approximately three times greater than that in 2005–2009 (3.38%).

Comparison of urban expansion using MODIS and Landsat data sets

Urban land spatial patterns in GFD from MODIS land cover product were compared with IUI classification results from Landsat imagery (Fig. 6). All these data were reprocessed to 1-km resolution and the same projection. We aggregated the original results of urban classification data from Landsat images as fractional cover information in 1-km grids. The results from Landsat images and socioeconomic data sets revealed rapid urbanization during 2000–2009, with dramatic changes in urban fringe areas. By contrast, minor fractional urban signals were detected from MODIS land cover data sets, in which the core urban

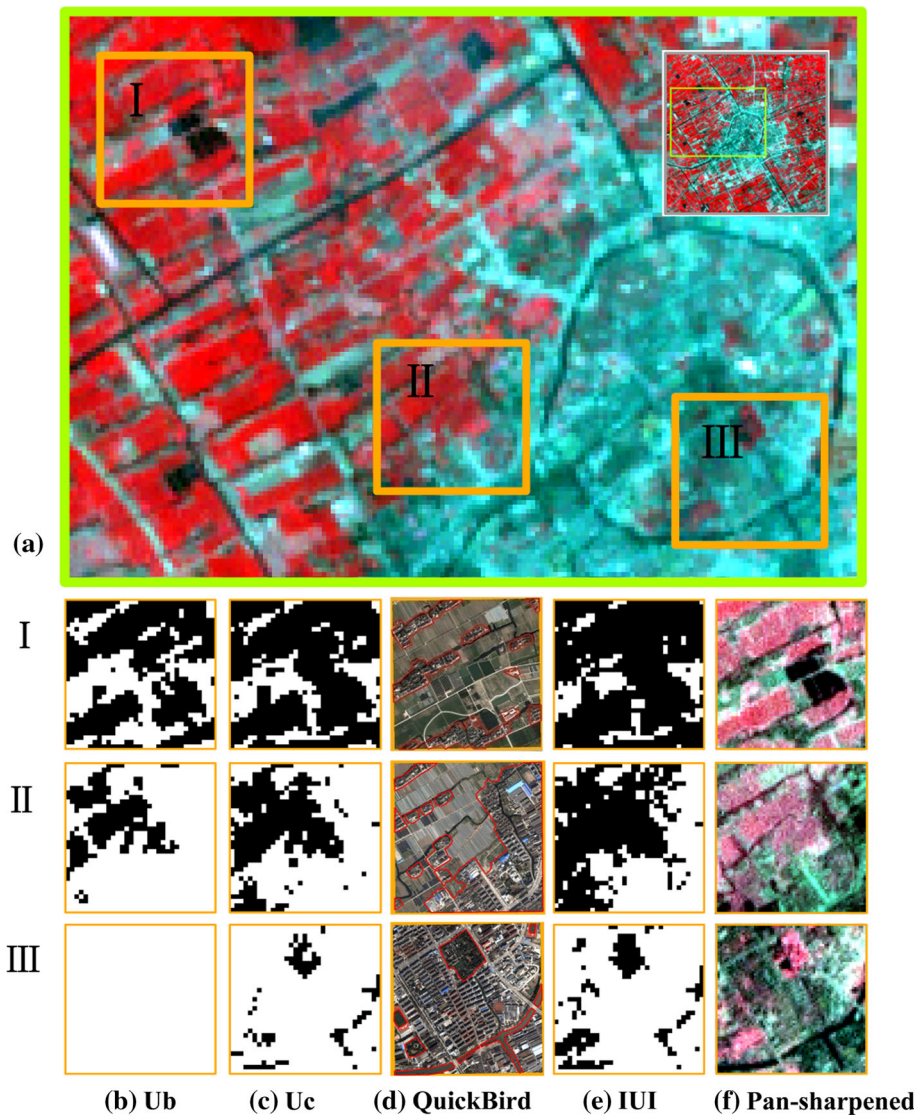

Fig. 4 Grids for accuracy assessments of IUI and existing methods at 1-km scale. **a** The false color composition (red:NIR, green:red and blue:green) of the Landsat ETM + image taken on April 27, 2000, located in Jiading District, Shanghai. Grid *I*, *II*, and *III* were chosen as exemplars in **a** to represent different level of urban development. Urban extents in column **b**, **c**, **e** were identified by methods of Ub, Uc, and IUI separately. Red outlines in column **d** were visual interpretation of urban areas in QuickBird image. Column **f** was false color composition of pan-sharpened imagery

areas were overestimated and rapid changes in the urban fringe were largely ignored.

To examine whether land cover products effectively captured urban expansion process, urban area derived from Landsat, MODIS land cover data sets, and census data were used to retrieve the urbanization rate, respectively (Table 4). Urbanization rate was defined as the rate of urban area growth per year. The rate was 0% from the MODIS data sets for GFD area, which showed that MODIS failed to capture recent urban expansion in the region. The rate for 2000–2005 was approximately three times as much as the rate for 2005–2009 from both Landsat data and census data. Census results were larger than Landsat results. It is possibly because census data were from the whole administrative divisions of Guangzhou, Foshan, and Dongguan cities. However, the rectangular grid of GFD area is not exactly the administrative boundary of census data.

Discussion

First, in commonly used climate models, the dominant category and urban fractions in a given pixel are used to characterize urban land cover. For dominant category, a coverage of built-up environment greater than 50% of a given landscape unit is defined as the threshold for an urban grid cell (Schneider et al. 2009). That is, those developing urban patches that cover 50% of the grid were taken as dominant underlying composition. For urban fractions, the proportions of urban areas within model grids are calculated to capture the detailed urban density and inner connections. Thus, both the dominant category and urban fractions need the information of fractional urban at the model grid resolution. In the accurate assessment at the 1-km scale, the grid II has a moderate level of development, with urban fractions approximately 50%. Urban fractions using the IUI and the QuickBird

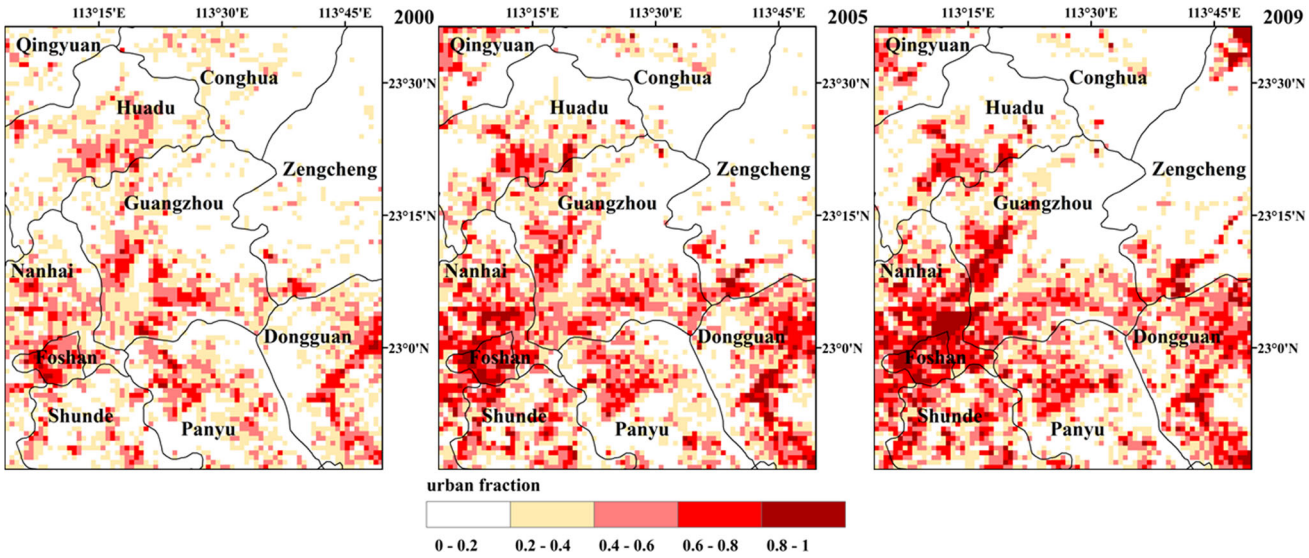

Fig. 5 Spatiotemporal change patterns of urban fractions in GFD area from 2000 to 2009. Urban fractions were calculated at an interval of 0.2

Table 3 Percentage of fractional urban change in the GFD area from 2000 to 2009

Interval	Urban fractions			Fractional urban change	
	2000 (%)	2005 (%)	2009 (%)	2000–2005 (%)	2005–2009 (%)
0–0.2	60.20	52.47	51.20	−7.73	−1.27
0.2–0.4	23.34	20.42	18.72	−2.92	−1.70
0.4–0.6	11.64	15.27	14.86	3.63	−0.41
0.6–0.8	4.45	9.55	11.26	5.10	1.71
0.8–1	0.37	2.29	3.96	1.92	1.67
Total	100	100	100	10.65	3.38

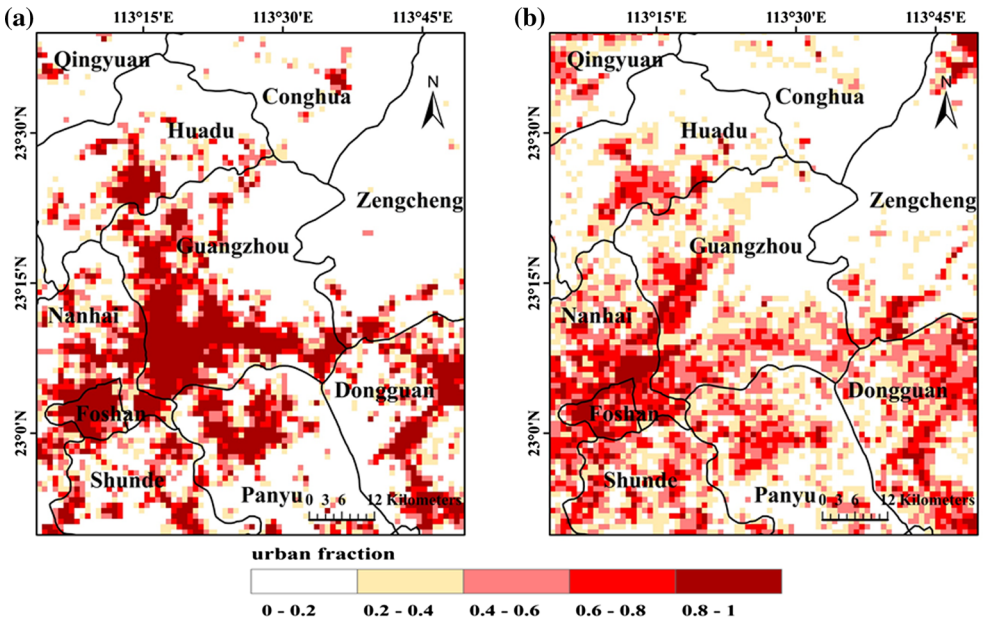

Fig. 6 Comparison of the urban land pattern in GFD area from MODIS land cover **a**, Landsat images **b** in 2009 at 1-km resolution

Table 4 Urban expansion comparison using MODIS and Landsat data in GFD area

Time	Urban area (km^2)		Urbanization rate[b] (%)		
	MODIS	Landsat	MODIS (%)	Landsat (%)	Census[a] (%)
2000	1807.75	1476.46	–	–	–
2005	1807.75	1868.07	0	4.8	15.5
2009	1807.75	1969.08	0	1.3	5.2

[a] Census data were collected from the Guangdong Province Statistical Yearbook

[b] Urbanization rate was defined as the rate of urban area growth per year:Urate $= \sqrt[n]{\frac{UA1}{UA2}} - 1$

where Urate is the annual urbanization rate, UA1 is the urban area in the previous period, UA2 is the urban area in the following period, and n is the interval between the two periods

image were both <50%, whereas urban fractions using Ub and Uc were much higher (Table 2). Therefore, both dominant category and urban fractions calculated by Ub and Uc had caused biases in urban underlying properties when applied in modeling. Moreover, in the comparison of urban expansion from MODIS and Landsat data sets, MODIS ignored fractional urban signals in the urban fringe and overestimated urban patches that cover 50% of the modeling grid.

Second, the total fractional urban change in 2000–2005 was almost three times greater than that in 2005–2009 (Table 3), suggesting that this area experienced high rates of urban expansion in 2000–2005, but the rates decelerated in 2005–2009. This indicates that the area has reached a mature stage of urbanization during the later five years. These urban dynamics are influenced by policy shifts, economic development, and demographic patterns (Seto et al. 2002). During the decade, China was implementing the 10th and 11th Five-Year Plans. The former plan gave China the first blueprint for the new century with main targets for economics and urbanization levels. The GFD area was developed during this period, with rapidly emerging satellite towns and expansion of core areas. These towns were not well connected to existing central urban areas (Zhang and Seto 2011). The latter plan, started from 2006, had a goal to enable disadvantaged groups and less developed regions in sharing the fruits of economic growth (Fan 2006). The government highlighted the role of urban clusters in fostering urbanization for the first time. These policy shifts might have contributed to the slowing down of urban development in this area, with extension in the core areas to satellite towns for developing an urban cluster. The high density (0.8–1) of fractional urban change indicates that the GFD area has become denser and packed with more continuous urban canopy in the decade. Such changing patterns of urban density and inner connections may potentially alter interactions between urban canopy and atmosphere and urban climate effects.

Conclusions

Reliable information on urban areas and change detection plays an important role in urban studies. The IUI can effectively capture better urban signals for different levels of urban fractions. The case study area in GFD experienced urban expansion during the decade, with fractional urban growth three times greater in 2000–2005 than in 2005–2009. The spatiotemporal patterns of urban expansion were presented with remarkable growth of satellite towns and core areas. We expect that better estimates of changing patterns of urban density and inner connections will help improve performance of models in capturing critical environmental feedbacks over expanding urban clusters.

Acknowledgements This study is supported by NSMC Foundation (201702QT007), National Key Research and Development Program of China (2016YFA0600303), and CAS Strategic Priority Research Program (XDA05090200). We thank Dr. Howard E. Epstein for valuable comments on our manuscript.

References

Bagan H, Yamagata Y (2012) Landsat analysis of urban growth: how Tokyo became the world's largest megacity during the last 40 years. Remote Sens Environ 127:210–222

Crawford TM, Stensrud DJ, Mora F, Merchant JW, Wetzel PJ (2001) Value of incorporating satellite-derived land cover data in MM5/PLACE for simulating surface temperatures. J Hydrometeorol 2:453–468

Dick HW, Rimmer PJ (1998) Beyond the third world city: the new urban geography of South-east Asia. Urban Stud 35:2303–2322

Fan CC (2006) China's eleventh five-year plan (2006–2010): from "getting rich first" to "common prosperity". Eurasian Geogr Econ 47:708–723

Fernando HJS, Klaić ZB, McCulley JL (Eds.) (2012) Interactions of global-warming and urban heat islands in different climate-zones, in National Security and Human Health Implications of Climate Change, pp. 49–60, Springer, Netherlands

Fischer EM, Oleson KW, Lawrence DM (2012) Contrasting urban and rural heat stress responses to climate change. Geophys Res Lett 39(3):419–420

Foley JA, DeFries R, Asner GP, Barford C, Bonan G, Carpenter SR, Chapin FS, Coe MT, Daily GC, Gibbs HK, Helkowski JH, Holloway T, Howard EA, Kucharik CJ, Monfreda C, Patz JA, Prentice IC, Ramankutty N, Snyder PK (2005) Global consequences of land use. Science 309:570–574

Friedl MA, McIver DK, Hodges JCF, Zhang XY, Muchoney D, Strahler AH, Woodcock CE, Gopal S, Schneider A, Cooper A, Bccini A, Gao F, Schaaf C (2002) Global land cover mapping from MODIS: algorithms and early results. Remote Sens Environ 83(83):287–302

Friedl MA, Sulla-Menashe D, Tan B, Schneider A, Ramankutty N, Sibley A, Huang XM (2010) MODIS Collection 5 global land cover: algorithm refinements and characterization of new datasets. Remote Sens Environ 114(1):168–182

Gao H, Jia G (2013) Assessing disagreement and tolerance of misclassification of satellite-derived land cover products used in WRF model applications. Adv Atmos Sci 30:125–141

Ge J, Qi J, Lofgren BM, Moore N, Torbick N, Olson JM (2007) Impacts of land use/cover classification accuracy on regional climate simulations. J Geophys Res-Atmos 112:1435–1440

Gong P, Wang J, Yu L, Zhao Y, Zhao Y, Liang L, Niu Z, Huang X, Fu H, Xu Y, Wang X, Cheng Q, Hu L, Yao W, Zhang H, Zhu P, Zhao Z, Zhang H, Zheng Y, Ji L, Zhang Y, Chen H, Yan A, Guo J, Yu L, Wang L, Liu X, Shi T, Zhu M, Chen Y, Yang G, Tang P, Xu B, Giri C, Clinton N, Zhu Z, Chen J, Chen J (2013) Finer resolution observation and monitoring of global land cover: first mapping results with Landsat TM and ETM + data. Int J Remote Sens 34(7):2607–2654

He C, Shi P, Xie D, Zhao Y (2010) Improving the normalized difference built-up index to map urban built-up areas using a semiautomatic segmentation approach. Remote Sens Lett 1(4):213–221

He Y, Jia G, Hu Y, Zhou Z (2013) Detecting urban warming signals in climate records. Adv Atmos Sci 30(4):1143–1153

Herold M, Roberts DA (2010) The Spectral Dimension. In: Rashed T, Jürgens C(ed).Urban remote sensing. Remote sensing of urban and suburban areas, remote sensing and digital image processing. Springer: Dordrecht, Vol 10, p 47–65

Hu Y, Hou M, Jia G, Zhang X, Xu R, He Y (2015a) Comparison of three different methods to identify fractional urban signals for improving climate modelling. Int J Remote Sens 36(12):3274–3292

Hu Y, Jia G, Hou M, Zhang X, Zheng F, Liu Y (2015b) The cumulative effects of urban expansion on land surface temperatures in metropolitan Jingjintang, China. J Geophys Res-Atmos 120:9932–9943

Jackson TL, Feddema JJ, Oleson KW, Bonan GB, Bauer JT (2010) Parameterization of urban characteristics for global climate modeling. Ann Assoc Am Geogr 100(4):848–865

Jia G, Xu R, Hu Y, Hu Y (2015) Multi-scale remote sensing estimates of urban fractions and road widths for regional models. Clim Change 129:543–554

Kalnay E, Cai M (2003) Impact of urbanization and land-use change on climate. Nature 423(6939):528–531

Normile D (2008) China's living laboratory in urbanization. Science 319(5864):740–743

Oleson KW, Bonan GB, Feddema J, Vertenstein M, Grimmond CSB (2008) An urban parameterization for a global climate model. Part I: Formulation and evaluation for two cities. J Appl Meteor Climatol 47(4):1038–1060

Peng S, Piao S, Ciais P, Friedlingstein P, Ottle C, Bréon F, Myneni R (2012) Surface urban heat island across 419 global big cities. Environ Sci Techno 46(2):696–703

Potere D, Schneider A, Angel S, Civco DL (2009) Mapping urban areas on a global scale: which of the eight maps now available is more accurate? Int J Remote Sens 30(24):6531–6558

Ren G, Zhou Y, Chu Z, Zhou J, Zhang A, Guo J, Liu X (2008) Urbanization effects on observed surface air temperature trends in North China. J Clim 21(6):1333–1348

Schneider A, Seto KC, Webster DR (2005) Urban growth in Chengdu, Western China: application of remote sensing to assess planning and policy outcomes. Environ Plann B 32(3):323–345

Schneider A, Friedl MA, Potere D (2009) A new map of global urban extent from MODIS satellite data. Environ Res Lett 4(4):44003–44033

Sertel E, Robock A, Ormeci C (2010) Impacts of land cover data quality on regional climate simulations. Int J Climatol 30(13):1942–1953

Seto KC, Woodcock CE, Song C, Huang X, Lu J, Kaufmann RK (2002) Monitoring land-use change in the Pearl River Delta using Landsat TM. Int J Remote Sens 23(10):1985–2004

Stocker TF, Plattner GK, Dahe Q (2013) Climate change 2013: The physical science basis, in Intergovernmental Panel on Climate Change, Working Group I Contribution to the IPCC Fifth Assessment Report (AR5), 1535 pp. Cambridge Univ. Press, New York

Sun C, Wu ZF, Lv ZQ, Yao N, Wei JB (2013) Quantifying different types of urban growth and the change dynamic in Guangzhou using multi-temporal remote sensing data. Int J Appl Earth OBS 21(1):409–417

Weng QH (2012) Remote sensing of impervious surfaces in the urban areas: requirements, methods, and trends. Remote Sens Environ 117(2):34–49

Xu HQ (2007) Extraction of urban built-up land features from Landsat imagery using a thematic-oriented index combination technique. Photogramm Eng Remote Sens 73(12):1381–1391

Zha Y, Gao J, Ni S (2003) Use of normalized difference built-up index in automatically mapping urban areas from TM imagery. Int J Remote Sens 24(3):583–594

Zhang Q, Seto KC (2011) Mapping urbanization dynamics at regional and global scales using multi-temporal DMSP/OLS nighttime light data. Remote Sens Environ 115(9):2320–2329